11th World Congress on Computational Mechanics (WCCM XI)
5th European Conference on Computational Mechanics (ECCM V)
6th European Conference on Computational Fluid Dynamics (ECFD VI)
E. Oñate, J. Oliver and A. Huerta (Eds)

NUMERICAL STUDY OF CONVERGENCE OF THE MASS REDISTRIBUTION METHOD FOR ELASTODYNAMIC CONTACT PROBLEMS

F. Dabaghi*, A. Petrov*, J. Pousin* and Y. Renard*

*Université de Lyon, CNRS, Institut Camille Jordan UMR5208, INSA–Lyon, F-69621 Villeurbanne, France, farshid.dabaghi@insa-lyon.fr, apetrov@math.univ-lyon1.fr, jerome.pousin@insa-lyon.fr, yves.renard@insa-lyon.fr

Key words: Elastodynamics, Signorini conditions, mass redistribution method, numerical convergence.

Abstract. This note deals with two and three–dimensional elastodynamic contact problems. An approximated solution combining the finite element and mass redistribution methods is exhibited. The mass redistribution method consists in a redistribution of the body mass such that the inertia at the contact node vanishes. Some numerical experiments using two time–integration methods, the Crank–Nicolson as well as backward Euler methods, highlighted the convergence properties of the mass redistribution method.

1 INTRODUCTION

This note aims to give some numerical results for the evolution of an elastic material being subjected to unilateral boundary conditions by employing the mass redistribution method introduced in [5]. The contact phenomena is modelled by using the so–called Signorini's boundary conditions in displacement, which are based on a linearization of the physically meaningful non penetrability of masses. A considerable engineering and mathematical literature is devoted to contact problems, however a few existence of solutions results has been established, the reader is referred to [9, 6]. Therefore a challenging task consists to elaborate efficient numerical methods able to approximate this problem. The present work adopt the approach consisting to remove the mass at the contact nodes which prevents the oscillations at the contact boundaries as already observed for the one dimensional elastodynamic contact problems in [2].

We consider an elastic bar vibrating vertically such that one end of this bar is free to move, as long as it does not hit a material obstacle, while the other end is clamped . The obstacle constrains the displacement of the extremity to be greater than or equal to 0. We have supposed that the material of the bar is a homogeneous and isotropic. Let us define $\Omega_d \subset \mathbb{R}^d$, $d = 2, 3$, the reference configuration of the bar and its boundary by $\partial\Omega_d \stackrel{\text{def}}{=}$

$\overline{\Gamma}_d^{\rm Dir} \cup \overline{\Gamma}_d^{\rm Neu} \cup \overline{\Gamma}_d^{\rm Sig}$ where $\Gamma_d^{\rm Dir}$, $\Gamma_d^{\rm Neu}$ and $\Gamma_d^{\rm Sig}$ denote the Dirichlet, Neumann and unilateral contact boundaries, respectively. In our case, we assume that $\Omega_2 \stackrel{\rm def}{=} [0, L_1] \times [0, L_2]$ and $\Omega_3 \stackrel{\rm def}{=} [0, L_1] \times [0, L_2] \times [0, L_3]$ together with $L_i > 0$, $i = 1, 2, 3$. We denote by $\boldsymbol{u}(\boldsymbol{x}, t)$ the displacement field at time $t \in [0, T]$, $T > 0$, of the material point of spatial coordinate $\boldsymbol{x} \in \Omega \subset \mathbb{R}^d$. Furthermore, let $\boldsymbol{f}(\boldsymbol{x}, t)$ be the density of external forces depending on time and space. The mathematical problem is formulated as follows:

$$\rho \boldsymbol{u}_{tt} - \operatorname{div} \boldsymbol{\sigma}(\boldsymbol{u}) = \boldsymbol{f} \quad \text{in} \quad \Omega_d \times (0, T), \tag{1}$$

where $\rho > 0$ is the mass density, $(\cdot)_t \stackrel{\rm def}{=} \frac{\partial (\cdot)}{\partial t}$ and $\boldsymbol{\sigma}(\boldsymbol{u})$ is the stress tensor with $\sigma_{ij}(\boldsymbol{u}) \stackrel{\rm def}{=} \mathcal{A}_{ijkl} \varepsilon_{kl}(\boldsymbol{u})$ where $\mathcal{A}_{ijkl}$ and $\varepsilon_{kl}(\boldsymbol{u}) \stackrel{\rm def}{=} \frac{1}{2}(\frac{\partial u_k}{\partial x_l} + \frac{\partial u_l}{\partial x_k})$ are the Hooke and strain tensors, respectively. Here the summation convention on repeated indices is used. Besides assuming isotropy of the material, the Hooke tensor is defined via Lamé constants λ and μ as $\mathcal{A}_{ijkl} \stackrel{\rm def}{=} \lambda \delta_{ij} \delta_{kl} + 2\mu \delta_{kl} \delta_{jk}$ where δ_{ij} denotes the Kronecker symbol. The Cauchy initial data are

$$\boldsymbol{u}(\cdot, 0) = \boldsymbol{u}^0 \quad \text{and} \quad \boldsymbol{u}_t(\cdot, 0) = \boldsymbol{v}^0 \quad \text{on} \quad \Omega_d, \tag{2}$$

and the boundary conditions are

$$\boldsymbol{u} = 0 \quad \text{on} \quad \Gamma_d^{\rm Dir} \times (0, T) \quad \text{and} \quad \boldsymbol{\sigma}(\boldsymbol{u})\boldsymbol{\nu} = 0 \quad \text{on} \quad \Gamma_d^{\rm Neu} \times (0, T), \tag{3a}$$

$$0 \geq \boldsymbol{\nu}^{\mathsf{T}} \boldsymbol{u} \perp \boldsymbol{\nu}^{\mathsf{T}} (\boldsymbol{\sigma}(\boldsymbol{u})\boldsymbol{\nu}) \leq 0 \quad \text{and} \quad \boldsymbol{\tau}^{\mathsf{T}} (\boldsymbol{\sigma}(\boldsymbol{u})\boldsymbol{\nu}) = 0 \quad \text{on} \quad \Gamma_d^{\rm Sig} \times (0, T), \tag{3b}$$

where $\boldsymbol{\nu}$ and $\boldsymbol{\tau}$ denote the outward unit normal and tangential vectors and $(\cdot)^{\mathsf{T}}$ is the transpose of a tensor. Here the orthogonality has the natural meaning; namely if we have enough regularity, it means that the product $\boldsymbol{\nu}^{\mathsf{T}} \boldsymbol{u} (\boldsymbol{\nu}^{\mathsf{T}} \boldsymbol{\sigma}(\boldsymbol{u}) \boldsymbol{\nu})$ vanishes almost everywhere at the contact boundary. If it is not the case, the above inequality is integrated on an appropriate set of test functions, leading to a weak formulation for the unilateral condition. Let us describe now the functional hypotheses on the data; if X is a space of scalar functions, the bold–face notation $\mathbf{X}$ denotes the space X^d. For the final result, we require the initial displacement $\boldsymbol{u}^0$ belongs to the $\mathbf{H}^1(\Omega_d)$ and satisfies the compatibility conditions, i.e. $\boldsymbol{u}^0 = 0$ on $\Gamma_d^{\rm Dir}$ and the initial velocity $\boldsymbol{v}^0$ belongs to $\mathbf{L}^2(\Omega_d)$. It is convenient to introduce the following notations: $\mathbf{V} \stackrel{\rm def}{=} \{\boldsymbol{u} \in \mathbf{H}^1(\Omega_d) : \boldsymbol{u} = 0 \text{ a.e. on } \Gamma_d^{\rm Sig}\}$, $\mathbf{H} \stackrel{\rm def}{=} \mathbf{L}^2(\Omega_d)$ and the convex set $\mathbf{K} \stackrel{\rm def}{=} \{\boldsymbol{u} \in \mathbf{L}^2(0, T; \mathbf{V}) : \boldsymbol{u}_t \in \mathbf{L}^2(0, T; \mathbf{H}), \boldsymbol{u}(\cdot, t) \in \mathbf{V} \text{ for a.e. } t, \boldsymbol{\nu}^{\mathsf{T}} \boldsymbol{u} \leq 0 \text{ a.e. on } \Gamma_d^{\rm Sig}\}$. Then the weak formulation associated to (1)–(3) is given by

$$\begin{cases} \text{find } \boldsymbol{u} : [0, T] \to \mathbf{K} \text{ such that} \\ \displaystyle\int_\Omega \rho \boldsymbol{u}_{tt} \cdot (\boldsymbol{v} - \boldsymbol{u}) \, \mathrm{d}\boldsymbol{x} + a(\boldsymbol{u}, \boldsymbol{v} - \boldsymbol{u}) \geq \int_\Omega \boldsymbol{f} \cdot (\boldsymbol{v} - \boldsymbol{u}) \, \mathrm{d}\boldsymbol{x}, \\ \text{for all } \boldsymbol{v} \in \mathbf{K}, \end{cases} \tag{4}$$

where $a(\boldsymbol{u}, \boldsymbol{v}) \stackrel{\rm def}{=} \int_\Omega \mathcal{A}_{ijkl} \varepsilon_{ij}(\boldsymbol{u}) \varepsilon_{kl}(\boldsymbol{v}) \, \mathrm{d}\boldsymbol{x}$. Observe that existence and uniqueness of the solution to (1)–(3) is still an open question. However, we have exhibited an approximated solution associated to (4) combining the finite element and mass redistribution methods.

The present note is organized as follows. A space semi–discretization based on a redistribution of mass is introduced in Section 2.1. Then two time–integration methods, namely the Crank–Nicolson and backward Euler methods are presented in Section 2.2. In Section 3, the comparison between the convergence rates for the solution and energy evolution obtained with and without the mass redistribution highlighted the efficiency of mass redistribution method.

2 THE FINITE ELEMENT APPROXIMATION OF PROBLEM

2.1 The semi–discretization in space

We introduce the semi–discrete problem in space associated to (4) by using a Lagrange finite element method defined on Ω_d. To this aim, we introduce the following notations: Let $\mathcal{T}_h$ be a regular mesh of Ω_d, $\mathbf{V}_h \stackrel{\text{def}}{=} \{\boldsymbol{v}_h \in \mathbf{C}^0(\Omega_d) : \boldsymbol{v}_h$ is piecewise linear over each $K_l \in \mathcal{T}_h \setminus \Gamma_d^{\text{Dir}}, \boldsymbol{v}_h = 0$ on $\Gamma_d^{\text{Dir}}\}$, n_d and n_c denote the number of degree of freedom and the number of nodes on Γ_d^{Sig}, respectively, and a_i, $i = 1, \ldots, n$, denotes the finite element nodes. The basis of $\mathbf{V}_h$ is defined using the set of shape functions $\boldsymbol{\varphi}_i \in \mathbf{V}_h$, $i = 1, \ldots, n_d$. Then the vector of degree of freedom of the finite element field $\boldsymbol{u}_h(\boldsymbol{x}, t)$ denoted by $\mathbf{U}_h = (u_1(t), \ldots, u_{n_d}(t))^{\mathsf{T}}$ such that $\boldsymbol{u}_h(\boldsymbol{x}, t) = \sum_{j=1}^{n_d} u_j(t)\boldsymbol{\varphi}_j(\boldsymbol{x})$. Let $M_{ij} = \rho \int_\Omega \boldsymbol{\varphi}_i \cdot \boldsymbol{\varphi}_j \, \mathrm{d}\boldsymbol{x}$, $S_{ij} = a(\boldsymbol{\varphi}_i, \boldsymbol{\varphi}_j)$ and $F_i = \int_\Omega \boldsymbol{f} \cdot \boldsymbol{\varphi}_i \, \mathrm{d}\boldsymbol{x}$ denote the components of the mass and stiffness matrices and the external forces, $i, j = 1, \ldots, n_d$, respectively. Furthermore let $\mathbf{B} \stackrel{\text{def}}{=} (\boldsymbol{\nu}_1, \ldots, \boldsymbol{\nu}_{n_c})^{\mathsf{T}}$ and $\boldsymbol{\lambda} \stackrel{\text{def}}{=} (\lambda_1, \ldots, \lambda_{n_c})^{\mathsf{T}}$. According to these notations, a finite element semi–discretization of (4) with nodal approximation of the contact condition is given by

$$\begin{cases} \text{find } \mathbf{U}_h : [0, T] \to \mathbb{R}^{n_d} \text{ and } \boldsymbol{\lambda} : [0, T] \to \mathbb{R}^{n_c} \text{ such that} \\ \mathbf{M}\mathbf{U}_{h,tt} + \mathbf{S}\mathbf{U}_h = \mathbf{F} + \mathbf{B}^{\mathsf{T}}\boldsymbol{\lambda} \text{ for a.e. } t \in [0, T], \\ 0 \geq \boldsymbol{\nu}_i^{\mathsf{T}}\mathbf{U}_h \perp \lambda_i \leq 0 \text{ for all } i \in \mathcal{I}_c \text{ and for a.e. } t \in [0, T], \\ \mathbf{U}_h(0) = \mathbf{U}_h^{\mathbf{0}} \quad \text{and} \quad \mathbf{U}_{h,t}(0) = \mathbf{V}_h^{\mathbf{0}}, \end{cases} \tag{5}$$

where $\mathcal{I}_c \stackrel{\text{def}}{=} \{i : a_i \in \Gamma_d^{\text{Sig}}\}$ and such that $(\boldsymbol{\nu}^{\mathsf{T}}\boldsymbol{u}_h)(a_i, t) = (\boldsymbol{\nu}_i^{\mathsf{T}}\mathbf{U}_h)(t)$ for all $i \in \mathcal{I}_c$ with $\boldsymbol{\nu}_i^{\mathsf{T}}\boldsymbol{\nu}_j = \delta_{i,j}$ and $\|\boldsymbol{\nu}_i\| = 1$, $\|\cdot\|$ being the Euclidean norm. Note that the Lagrange multipliers are indeed the nodal contact equivalent forces. The discrete energy associated to problem (5) is given by

$$\mathcal{E}_h(t) = \frac{1}{2}(\mathbf{U}_{h,t}^{\mathsf{T}}\mathbf{M}\mathbf{U}_{h,t} + \mathbf{U}_h^{\mathsf{T}}\mathbf{S}\boldsymbol{U}_h - \mathbf{U}_{h,t}^{\mathsf{T}}\mathbf{F})(t). \tag{6}$$

The multiplicity of the solution to Problem (5) allow us to conclude that the considered problem is ill–posed, the reader is referred to [10, 11, 5]) for further details. An alternative approach to the standard discretization presented above is to consider the mass redistributions method which consists to replace the mass matrix $\mathbf{M}$ in by a modified mass matrix $\mathbf{M}^{\text{mod}}$ defined by $M_{ij}^{\text{mod}} \stackrel{\text{def}}{=} \rho \int_{\Omega_{d,h}^{\text{mod}}} \boldsymbol{\varphi}_i \cdot \boldsymbol{\varphi}_j \, \mathrm{d}\boldsymbol{x}$ with $\Omega_{d,h}^{\text{mod}} = \{K_l : K_l \in \mathcal{T}_h, K_l \cap \Gamma_d^{\text{Sig}} = \emptyset\}$ for all $i, j = 1, \ldots, n_d$. Note that $\ker(\mathbf{M}^{\text{mod}}) = \boldsymbol{\mathcal{N}}$ where $\boldsymbol{\mathcal{N}} \stackrel{\text{def}}{=} \text{span}\{\boldsymbol{\nu}_1, \ldots, \boldsymbol{\nu}_{n_c}\}$ denotes the

space spanned by $\boldsymbol{\nu}_i$ for $i \in \mathcal{I}_c$. Thus employing the identity $\mathbf{U}_h(t) = \mathbf{U}_h^{\boldsymbol{\mathcal{N}}}(t) + \mathbf{U}_h^{\boldsymbol{\mathcal{N}}^\perp}(t)$ where $\boldsymbol{\mathcal{N}}^\perp$ is the orthogonal complement of $\boldsymbol{\mathcal{N}}$, and replacing the mass matrix $\mathbf{M}$ by the modified one $\mathbf{M}^{\text{mod}}$ in (5), we get

$$\begin{cases} \text{find } \mathbf{U}_h^{\boldsymbol{\mathcal{N}}} : [0,T] \to \boldsymbol{\mathcal{N}}, \mathbf{U}_h^{\boldsymbol{\mathcal{N}}^\perp} : [0,T] \to \boldsymbol{\mathcal{N}}^\perp \text{ and } \boldsymbol{\lambda} : [0,T] \to \mathbb{R}^{n_c} \text{ such that} \\ \mathbf{M}^{\text{mod}} \mathbf{U}_{h,tt}^{\boldsymbol{\mathcal{N}}^\perp} + \mathbf{S}(\mathbf{U}_h^{\boldsymbol{\mathcal{N}}} + \boldsymbol{U}_h^{\boldsymbol{\mathcal{N}}^\perp}) = \mathbf{F} + \mathbf{B}^\mathsf{T} \boldsymbol{\lambda} \text{ for a.e. } t \in [0,T], \\ 0 \geq \boldsymbol{\nu}_i^\mathsf{T} \mathbf{U}_h^{\boldsymbol{\mathcal{N}}} \perp \lambda_i \leq 0 \text{ for all } i \in \mathcal{I}_c \text{ and for a.e. } t \in [0,T], \\ \mathbf{U}_h(0) = \mathbf{U}_h^0 \quad \text{and} \quad \mathbf{U}_{h,t}(0) = \mathbf{V}_h^0. \end{cases} \tag{7}$$

Existence and uniqueness of solution associated to (7) as well as the energy balance have been established in [1, 5]. Furthermore, the convergence of the mass redistribution method is established in the one–dimensional case in [1] confirming the observations already made in [2]. Note that the convergence of the mass redistribution is still an open problem in the higher dimension space.

2.2 The time integration methods

We introduce now the time discretization. In order to fix the notations, let the time interval $[0,T]$ be divided by $n+1$ discrete time–points such that $0 = t_0 < t_1 < \ldots < t_n = T$. Furthermore the discrete quantities $\mathbf{U}_h^n$, $\mathbf{U}_{h,t}^n$, $\mathbf{U}_{h,tt}^n$ and $\boldsymbol{\lambda}^n$ are assumed to be given by algorithmic approximations of the displacement $\mathbf{U}_h(t_n)$, the velocity $\mathbf{U}_{h,t}(t_n)$, the acceleration $\mathbf{U}_{h,tt}(t_n)$ and the Lagrange multiplier $\boldsymbol{\lambda}(t_n)$, respectively. Some time–stepping schemes allowing to obtain an approximated solution to Problem (5) are introduced below and their efficiency is discussed and analyzed in the next section.

One of the most popular method in the community of computational mechanics is the Crank–Nicolson method. This method is second–order consistent and unconditionally stable in the unconstrained case. Furthermore, the total energy of the discrete evolution is preserved, for the purely elastic case, see [8]. However, the situation is quite different in the contact constraints case, the order of accuracy is degraded, for further details, the reader is referred to [4, 7, 3]. Notice that the discrete evolution associated to (5) can be described by the finite difference equations:

$$\begin{cases} \text{find } \mathbf{U}_h^{n+1} : [0,T] \to \mathbb{R}^{n_d} \text{ and } \boldsymbol{\lambda}^{n+1} : [0,T] \to \mathbb{R}^{n_c} \text{ such that} \\ \mathbf{U}_h^{n+1} = \mathbf{U}_h^n + \Delta t \mathbf{U}_{h,t}^n + \dfrac{\Delta t^2}{4}(\mathbf{U}_{h,tt}^n + \mathbf{U}_{h,tt}^{n+1}), \\ \mathbf{U}_{h,t}^{n+1} = \mathbf{U}_{h,t}^n + \dfrac{\Delta t}{2}(\mathbf{U}_{h,tt}^n + \mathbf{U}_{h,tt}^{n+1}), \\ \mathbf{M}\mathbf{U}_{h,tt}^{n+1} + \mathbf{S}\mathbf{U}_h^{n+1} = \mathbf{F}^{n+1} + \mathbf{B}^\mathsf{T} \boldsymbol{\lambda}^{n+1}, \\ 0 \geq \boldsymbol{\nu}_i^\mathsf{T} \mathbf{U}_h^{n+1} \perp \lambda_i^{n+1} \leq 0 \text{ for all } i \in \mathcal{I}_c, \end{cases} \tag{8}$$

where Δt is a given times step and $\mathbf{U}_h^0$, $\mathbf{U}_{h,t}^0$ and $\boldsymbol{\lambda}^0$ are given. Therefore we observe that

(8) leads to the following algorithm:

$$\begin{cases} \text{find } \mathbf{U}_h^{n+1} : [0,T] \to \mathbb{R}^{n_d} \text{ and } \boldsymbol{\lambda}^{n+1} : [0,T] \to \mathbb{R}^{n_c} \text{ such that} \\ \left(\dfrac{4\mathbf{M}}{\Delta t^2}+\mathbf{S}\right)\mathbf{U}_h^{n+1} = \dfrac{4\mathbf{M}}{\Delta t^2}(\mathbf{U}_h^n+\Delta t\mathbf{U}_{h,t}^{n+1}) + \mathbf{M}\mathbf{U}_{h,tt}^n + \mathbf{F}^{n+1} + \mathbf{B}^{\mathsf{T}}\boldsymbol{\lambda}^{n+1}, \\ 0 \geq \boldsymbol{\nu}_i^{\mathsf{T}}\mathbf{U}_h^{n+1} \perp \lambda_i^{n+1} \leq 0 \text{ for all } i \in \mathcal{I}_c, \end{cases} \tag{9}$$

The energy evolution is defined by $\Delta\mathcal{E}_h^n \stackrel{\text{def}}{=} \mathcal{E}_h^{n+1} - \mathcal{E}_h^n$, where $\mathcal{E}_h^n$ is supposed to be given by an algorithmic approximation of the energy $\mathcal{E}_h(t_n)$. Thus the energy evolution associated to (8) by using the Crank–Nicolson method is $\Delta\mathcal{E}_h^n = -\frac{1}{2}(\mathbf{U}_h^{n+1}-\mathbf{U}_h^n)^{\mathsf{T}}\mathbf{B}^{\mathsf{T}}(\boldsymbol{\lambda}^n+\boldsymbol{\lambda}^{n+1})$.

Another time integration method to approach the semi–discrete problem (5) consists to use the backward Euler method which gives us the following discrete evolution associated to (5):

$$\begin{cases} \text{find } \mathbf{U}_h^{n+1} : [0,T] \to \mathbb{R}^{n_d} \text{ and } \boldsymbol{\lambda}^{n+1} : [0,T] \to \mathbb{R}^{n_c} \text{ such that} \\ \mathbf{U}_h^{n+1} = \mathbf{U}_h^n + \Delta t\mathbf{U}_{h,t}^{n+1}, \\ \mathbf{U}_{h,t}^{n+1} = \mathbf{U}_{h,t}^n + \Delta t\mathbf{U}_{h,tt}^{n+1}, \\ \mathbf{M}\mathbf{U}_{h,tt}^{n+1} + \mathbf{S}\mathbf{U}_h^{n+1} = \mathbf{F}^{n+1} + \mathbf{B}^{\mathsf{T}}\boldsymbol{\lambda}^{n+1}, \\ 0 \geq \boldsymbol{\nu}_i^{\mathsf{T}}\mathbf{U}_h^{n+1} \perp \lambda_i^{n+1} \leq 0 \text{ for all } i \in \mathcal{I}_c, \end{cases} \tag{10}$$

where $\mathbf{U}_h^0$, $\mathbf{U}_{h,t}^0$ and $\boldsymbol{\lambda}^0$ are given. Therefore notice that (10) enables us to infer the following algorithm:

$$\begin{cases} \text{find } \mathbf{U}_h^{n+1} : [0,T] \to \mathbb{R}^{n_d} \text{ and } \boldsymbol{\lambda}^{n+1} : [0,T] \to \mathbb{R}^{n_c} \text{ such that} \\ \left(\dfrac{4\mathbf{M}}{\Delta t^2}+\mathbf{S}\right)\mathbf{U}_h^{n+1} = \dfrac{4\mathbf{M}}{\Delta t^2}(\mathbf{U}_h^n+\Delta t\mathbf{U}_{h,t}^{n+1}) + \mathbf{F}^{n+1} + \mathbf{B}^{\mathsf{T}}\boldsymbol{\lambda}^{n+1}, \\ 0 \geq \boldsymbol{\nu}_i^{\mathsf{T}}\mathbf{U}_h^{n+1} \perp \lambda_i^{n+1} \leq 0 \text{ for all } i \in \mathcal{I}_c, \end{cases} \tag{11}$$

In this case, the energy evolution associated to (10) reads as $\Delta\mathcal{E}_h^n = -\frac{1}{2}(\mathbf{U}_{h,t}^{n+1} - \mathbf{U}_{h,t}^n)^{\mathsf{T}}\mathbf{M}$ $(\mathbf{U}_{h,t}^{n+1} - \mathbf{U}_{h,t}^n) - \frac{1}{2}(\mathbf{U}_h^{n+1} - \mathbf{U}_h^n)^{\mathsf{T}}\mathbf{S}(\mathbf{U}_h^{n+1} - \mathbf{U}_h^n) - \Delta t(\mathbf{U}_h^{n+1} - \mathbf{U}_h^n)^{\mathsf{T}}\mathbf{B}^{\mathsf{T}}\boldsymbol{\lambda}^{n+1}$. The reader is referred to [2, Appendix] where the energy evolutions associated to the Crank–Nicolson and backward Euler methods are justified. Note that $\mathbf{U}_{h,tt}$ appears on the right hand side of (11) which is not the case in (9) implying that the backward Euler method is dissipative and stable.

3 NUMERICAL EXPERIMENTS

The parameters used in the numerical simulations are $\Omega_2 = [0, 0.1] \times [0, 1]$, $\Omega_3 = [0, 0.1]\times[0, 0.1]\times[0, 1]$, $\rho = 1$, the Lamé parameters $\lambda = 0.25$ and $\mu = 0.5$, $u(x_1, 1, t) = 0.2$, $x_1 \in [0, 0.1]$ for dimension two and $u(x_1, x_2, 1, t) = 0.2$, $(x_1, x_2) \in [0, 0.1] \times [0, 0.1]$ for dimension three. The bar is undeformed at $t = 0$ ant it is located at the distance of 0.2 from a rigid obstacle. The bar starts to move toward the rigid obstacle with an initial velocity equal to -0.5 (vertical direction) and without any external forces. Note that

we used the square and cubic meshes with square and cube elements for two and three dimensional case, respectively.

The Crank–Nicolson and backward Euler methods are used below to compute $(\mathbf{U}_h^n, \boldsymbol{\lambda}^n)$. These computations are performed for the standard mass matrix $\mathbf{M}$ as well as for the modified mass matrix $\mathbf{M} = \mathbf{M}^{\text{mod}}$. Contrary to the one–dimensional elastodynamic contact problem treated in [2], we were not able here to exhibit an explicit solution associated to (1)–(3). However the explicit solution denoted by $(\mathbf{U}, \boldsymbol{\lambda})$ can be approximated by $(\mathbf{U}_h^n, \boldsymbol{\lambda}^n)$ by taking Δt and Δx very small. Therefore $(\mathbf{U}, \boldsymbol{\lambda})$ plays the role of an explicit solution in the numerical simulations presented below. Similarly the energy $\mathcal{E}$ is assumed to be equal to $\mathcal{E}_h^n$ for Δt and Δx chosen sufficiently small. The numerical simulations were performed by employing the finite element library Getfem++ (see [12]).

3.1 The Crank–Nicolson scheme

We focus first on the two–dimensional elastodynamic contact problem for which an approximated solution at the contact nodes as well as some convergence curves were obtained. More precisely, some spurious oscillations can be observed for the normal displacement at the contact nodes and the Lagrange multiplier, both of them are computed by using the standard mass matrix after the contact takes place, see Figure 1. These oscillations do not exist in the case where the standard mass matrix is replaced by the modified one, see Figure 1. Note that the scaling in space is different for the Lagrange multiplier evaluated by using standard and modified mass matrices. The scheme with the standard mass matrix is unstable with a rapidly growing energy while the one with the modified mass matrix is almost conservative as the space Δx and time Δt steps tend to 0. The error curves for $(\mathbf{U}_h^n, \boldsymbol{\lambda}^n)$ in Figure 3 highlighted that the norms $\|\mathbf{U}_h^n - \mathbf{U}\|_{\mathbf{L}^2(0,T;\mathbf{V})}$, and $\|\boldsymbol{\lambda}^n - \boldsymbol{\lambda}\|_{\mathbf{L}^2(0,T)}$ converge to 0 when $\mathbf{M} = \mathbf{M}^{\text{mod}}$ as n tends to $+\infty$, which is unfortunately not the case for the standard mass matrix, while the norms $\|\mathbf{U}_h^n - \mathbf{U}\|_{\mathbf{L}^p(0,T;\mathbf{H})}$, $p = 2, \infty$, converges to 0 as n tends to 0 in the both cases. Furthermore, we may observe that Figure 2 shows that the norm $\|\mathcal{E}_h^n - \mathcal{E}\|_{\mathrm{L}^p(0,T)}$, $p = 2, +\infty$, converges when $\mathbf{M} = \mathbf{M}^{\text{mod}}$ while this norm diverges when the standard mass matrix is considered.

The evolution of the von Mises stress in a three–dimensional bar by using the standard and modified mass matrices is represented in Figures 4 and 5. Note that the von Mises stress is usually used to predict yielding of materials under any loading condition from results of simple uniaxial tensile test. As in the two–dimensional case, some spurious oscillations can be observed in a neighborhood of the contact nodes in the case where the standard matrix is considered. Then these oscillations propagated along the bar (see Figure 4). In the case where the standard mass matrix is replaced by the modified one, these oscillations do not exist anymore (see Figure 5).

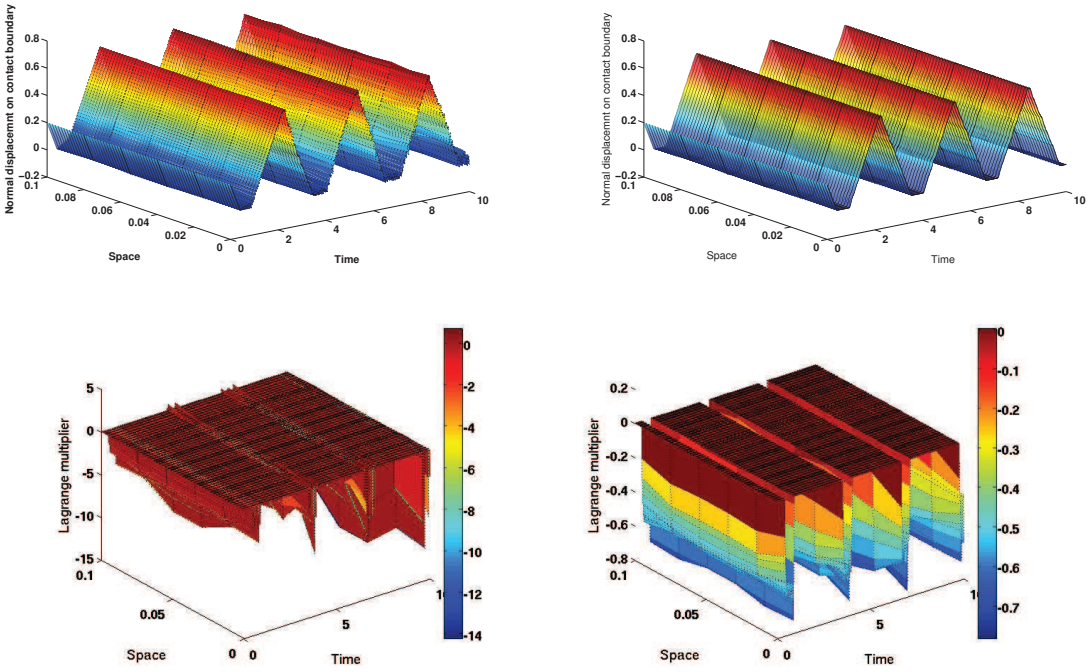

Figure 1: Approximated solutions obtained by using the standard (left) and modified (right) mass matrices in the contact node.

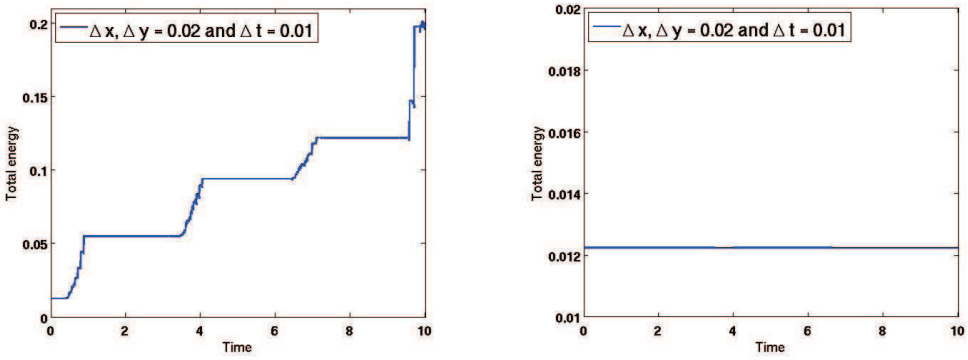

Figure 2: Energy associated to the approximated solution for the standard (left) and modified (right) mass matrices.

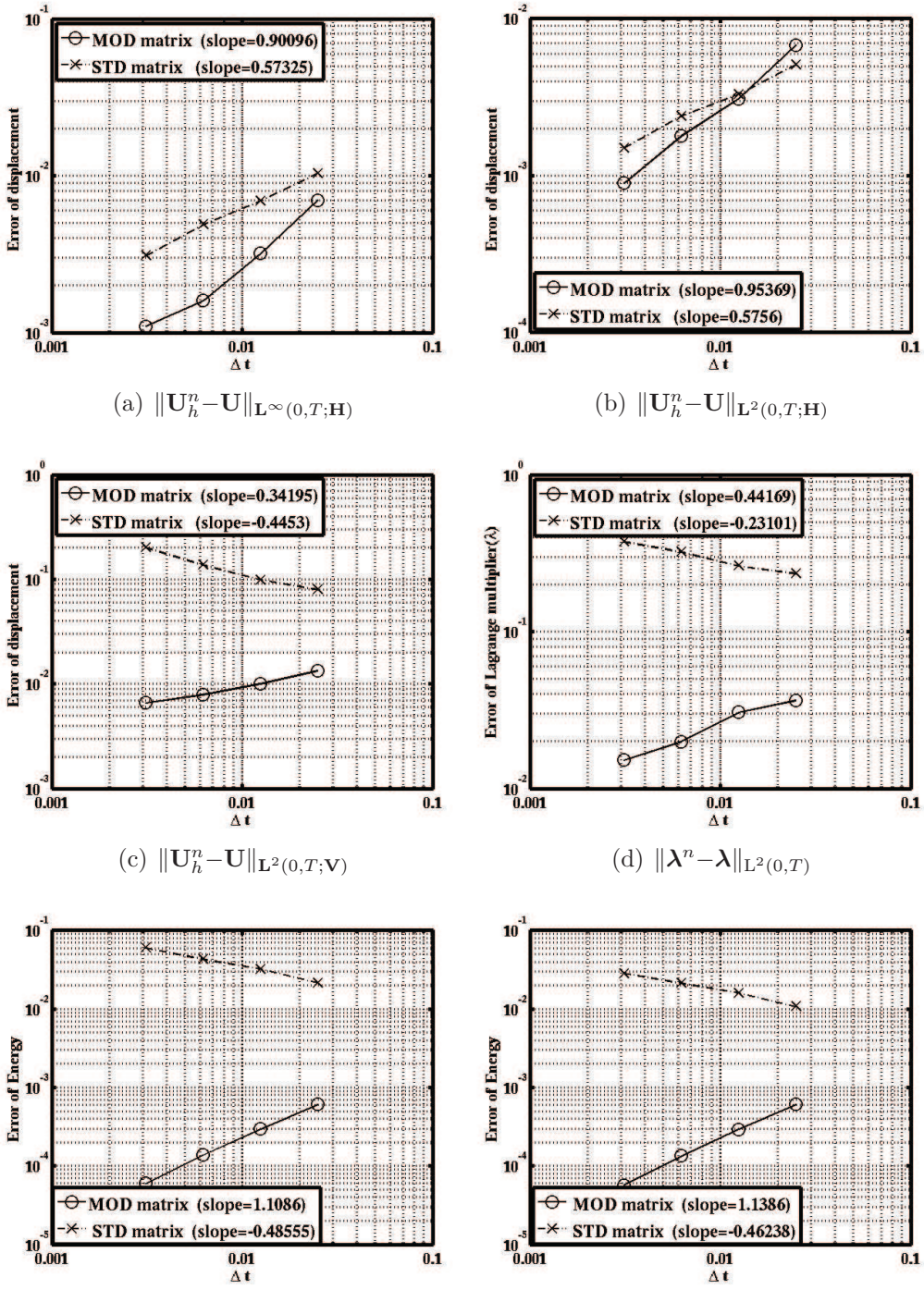

(a) $\|\mathbf{U}_h^n - \mathbf{U}\|_{\mathbf{L}^\infty(0,T;\mathbf{H})}$ (b) $\|\mathbf{U}_h^n - \mathbf{U}\|_{\mathbf{L}^2(0,T;\mathbf{H})}$

(c) $\|\mathbf{U}_h^n - \mathbf{U}\|_{\mathbf{L}^2(0,T;\mathbf{V})}$ (d) $\|\boldsymbol{\lambda}^n - \boldsymbol{\lambda}\|_{\mathrm{L}^2(0,T)}$

(e) $\|\mathcal{E}_h - \mathcal{E}\|_{\mathrm{L}^\infty(0,T)}$ (f) $\|\mathcal{E}_h - \mathcal{E}\|_{\mathrm{L}^2(0,T)}$

Figure 3: Comparison of the convergence curves obtained by the modified and standard mass matrices with square elements and $\frac{\Delta x}{\Delta t} = 2$

.

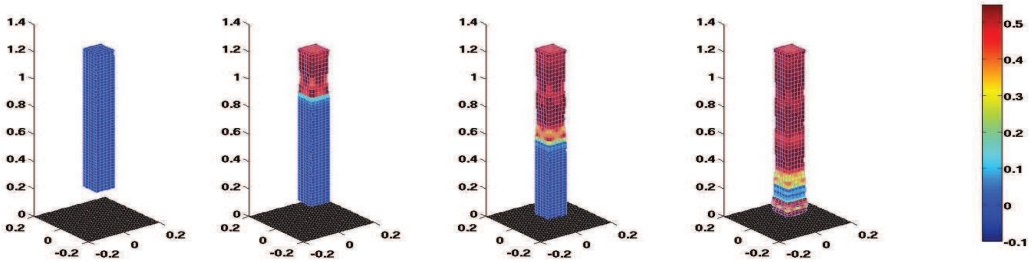

(a) t=0 (b) t=0.2 (c) t=0.4 (d) t=0.6

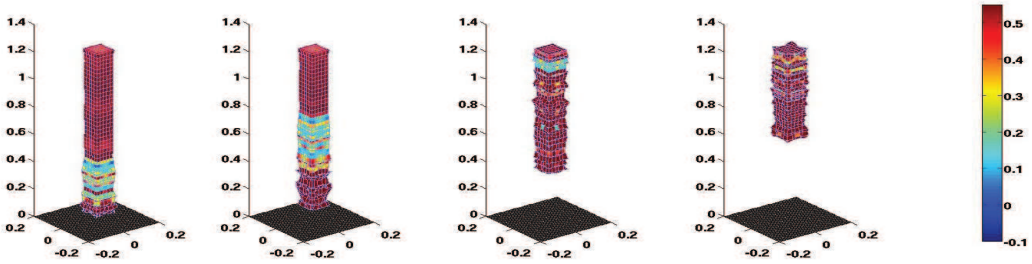

(e) t=0.8 (f) t=1 (g) t=1.5 (h) t=2

Figure 4: The evolution of the von Mises stress in a bar by using the standard mass matrix.

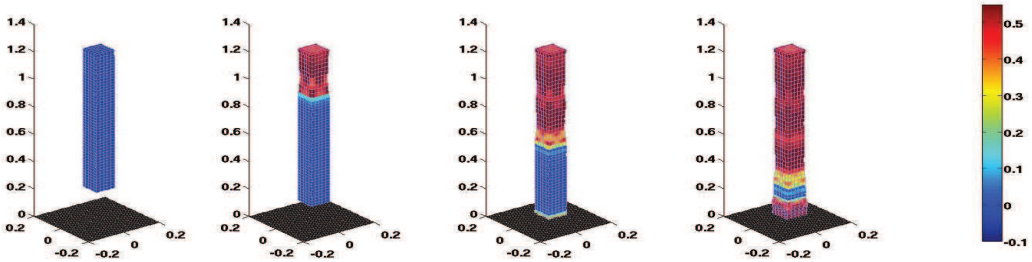

(a) t=0 (b) t=0.2 (c) t=0.4 (d) t=0.6

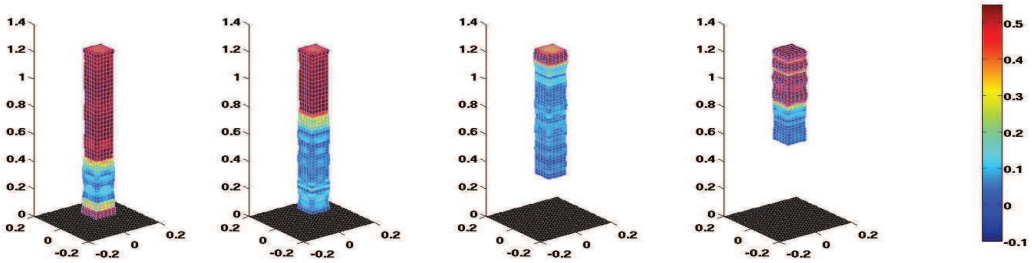

(e) t=0.8 (f) t=1 (g) t=1.5 (h) t=2

Figure 5: The evolution of the von Mises stress in a bar by using the modified mass matrix.

3.1.1 The backward Euler method

The normal displacement at the contact nodes and the Lagrange multiplier obtained by using the standard mass as well as modified mass matrices do not oscillate (see Figure 6) as it can be observed for the Crank–Nicolson method. Furthermore, the error curves converge for both methods (see Figure 8) and the energy are almost the same (see Figure 7).

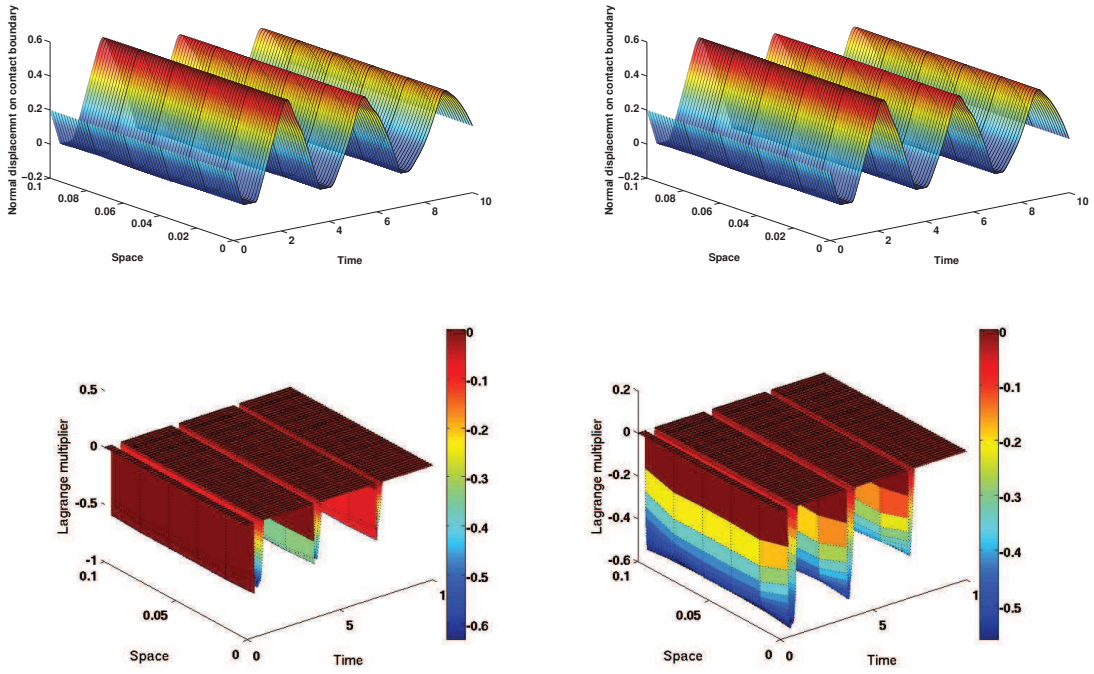

Figure 6: Approximated solutions obtained by using the standard (left) and modified (right) mass matrices in the contact node.

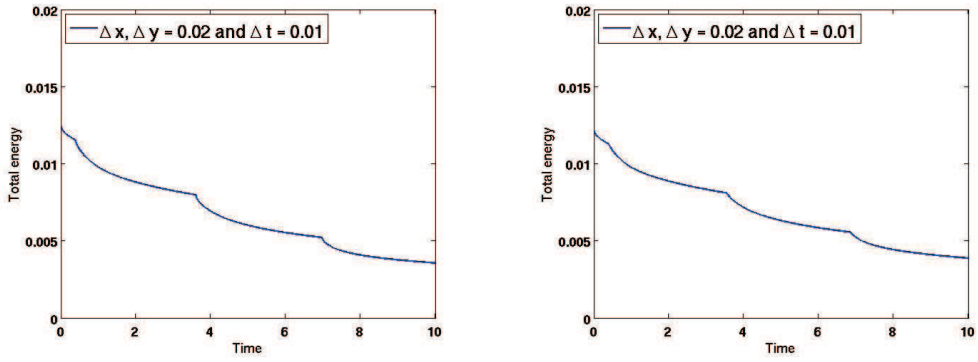

Figure 7: Energy associated to the approximated solution for the standard (left) and modified (right) mass matrices.

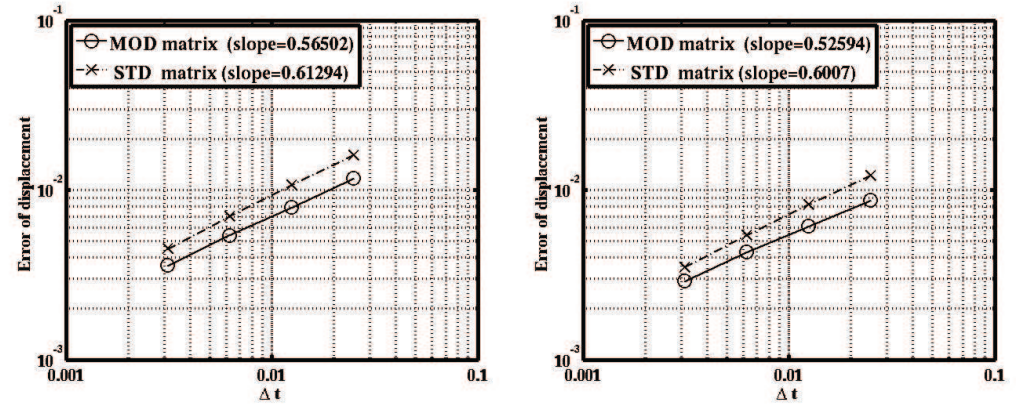

(a) $\|\mathbf{U}_h^n - \mathbf{U}\|_{\mathbf{L}^\infty(0,T;\mathbf{H})}$

(b) $\|\mathbf{U}_h^n - \mathbf{U}\|_{\mathbf{L}^2(0,T;\mathbf{H})}$

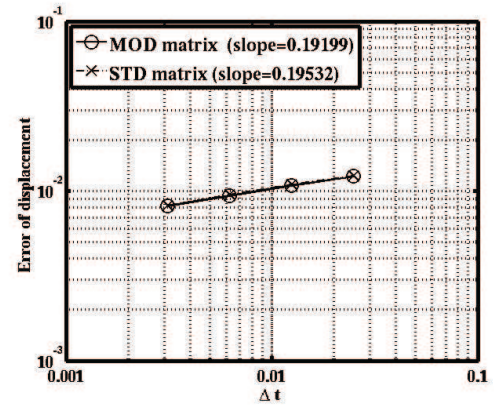

(c) $\|\mathbf{U}_h^n - \mathbf{U}\|_{\mathbf{L}^2(0,T;\mathbf{V})}$

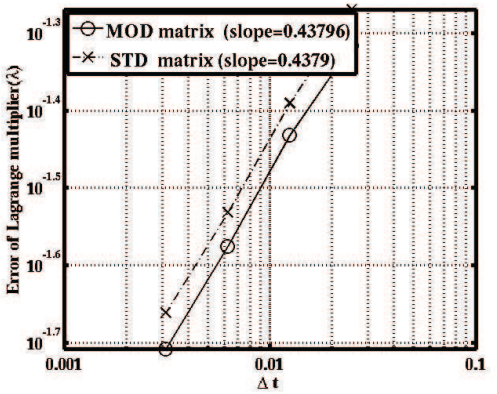

(d) $\|\lambda^n - \lambda\|_{\mathrm{L}^2(0,T)}$

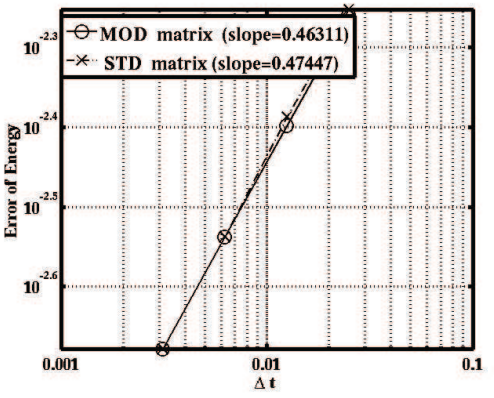

(e) $\|\mathcal{E}_h - \mathcal{E}\|_{\mathrm{L}^\infty(0,T)}$

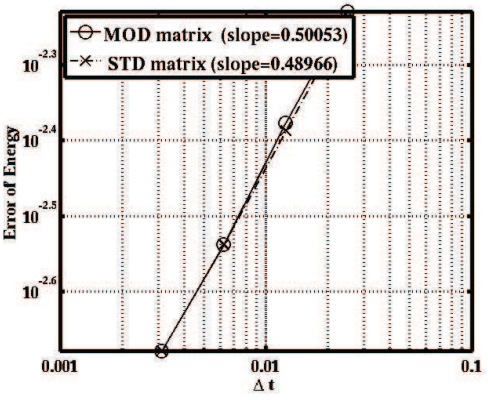

(f) $\|\mathcal{E}_h - \mathcal{E}\|_{\mathrm{L}^2(0,T)}$

Figure 8: Comparison of the convergence curves obtained by the modified and standard mass matrices with square elements $\frac{\Delta x}{\Delta t} = 2$

.

Acknowledgments The support of the AVCR–CNRS "Mathematical and numerical analysis of contact problems for materials with memory" grant is gratefully acknowledged.

REFERENCES

[1] F. Dabaghi, A. Petrov, J. Pousin, and Y. Renard. Convergence of mass redistribution method for the wave equation with a unilateral constraint at the boundary. *ESAIM: Mathematical Modelling and Numerical Analysis*.

[2] F. Dabaghi, A. Petrov, J. Pousin, and Y. Renard. Numerical approximations of elastodynamic contact problems based on mass redistribution method. *Submitted*, hal–00917450, 2013.

[3] E. Grosu and I. Harari. Stability of semidiscrete formulations for elastodynamics at small time steps. *Finite Elem. Anal. Des.*, 43(6-7), 533–542, 2007.

[4] T. J. R. Hughes. *The finite element method*. Prentice Hall Inc., Englewood Cliffs, NJ, 1987. Linear static and dynamic finite element analysis, With the collaboration of Robert M. Ferencz and Arthur M. Raefsky.

[5] H. B. Khenous, P. Laborde, and Y. Renard. Mass redistribution method for finite element contact problems in elastodynamics. *Eur. J. Mech. A Solids*, 27(5), 918–932, 2008.

[6] J. U. Kim. A boundary thin obstacle problem for a wave equation. *Comm. Partial Differential Equations*, 14(8–9):1011–1026, 1989.

[7] S. Krenk. Energy conservation in Newmark based time integration algorithms. *Comput. Methods Appl. Mech. Engrg.*, 195(44-47), 6110–6124, 2006.

[8] T. A. Laursen. Computational contact and impact mechanics. Fundamentals of modeling interfacial phenomena in nonlinear finite element analysis. *Springer-Verlag, Berlin, Heidelberg, New York*, 2003.

[9] G. Lebeau and M. Schatzman. A wave problem in a half–space with a unilateral constraint at the boundary. *J. Differential Equations*, 53(3):309–361, 1984.

[10] J.-J. Moreau. Liaisons unilatérales sans frottement et chocs inélastiques. *C. R. Acad. Sci. Paris Sér. II Méc. Phys. Chim. Sci. Univers Sci. Terre*, 296(19), 1473–1476, 1983.

[11] L. Paoli. Time discretization of vibro-impact. *R. Soc. Lond. Philos. Trans. Ser. A Math. Phys. Eng. Sci.*, 359(1789), 2405–2428, 2001. Non-smooth mechanics.

[12] Y. Renard and J. Pommier. Getfem++. An Open Source generic C++ library for finite element methods, *http://home.gna.org/getfem.*